Cancer Letters 465 (2019) 82–93

Contents lists available at ScienceDirect

Cancer Letters

journal homepage: www.elsevier.com/locate/canlet

A pharmacogenomic analysis using L1000CDS^2 identifies BX-795 as a potential anticancer drug for primary pancreatic ductal adenocarcinoma cells

Eun A Choi[a], Yeon-Sook Choi[a], Eun Ji Lee[a], Shree Ram Singh[b], Song Cheol Kim[c,**], Suhwan Chang[a,d,*]

[a] Department of Biomedical Sciences, University of Ulsan College of Medicine, Asan Medical Center, Seoul, 05505, Republic of Korea
[b] Basic Research Laboratory, National Cancer Institute, Frederick, MD, 21702, USA
[c] Department of Surgery, University of Ulsan College of Medicine, Asan Medical Center, Seoul, 05505, Republic of Korea
[d] Department of Physiology, University of Ulsan College of Medicine, Asan Medical Center, Seoul, 05505, Republic of Korea

ARTICLE INFO

Keywords:
Pancreatic cancer
L1000CDS2
BX-795
Pancreatic ductal adenocarcinoma cell
Patient-derived xenograft model

ABSTRACT

Pancreatic cancer is one of the leading causes of cancer death, mainly due to the absence of early diagnostic tool and effective therapeutic agents. To identify an effective therapeutic agent for pancreatic ductal adenocarcinoma cells (PDAC), we used 10 Gene Expression Omnibus (GEO) data sets and L1000CDS^2 pharmacogenetic search tool and obtained chemical "perturvants" that were predicted to reverse the abnormal gene expression changes in PDAC. Among 20 initial candidates, we measured IC_{50} for six compounds and identified BX-795, PDK1/TBK1 inhibitor, as a therapeutic candidate. We found that BX-795 inhibits primary PDAC cell proliferation more effectively than normal cells. Following molecular analysis revealed that BX-795 down-regulates mTOR-GSK3β pathway and trigger apoptosis. Moreover, we found that BX-795 suppresses primary PDAC cell migration via downregulation of Snail and Slug. Finally, efficacy test in patient-derived xenograft model of PDAC showed BX-795 can inhibit in vivo tumor growth as efficient as gemcitabine and a combination with trametinib further suppresses tumor growth. Collectively, these results demonstrate the BX-795 as an effective therapeutic candidate for PDAC treatment.

1. Introduction

Pancreatic cancer is a fatal disease with extremely high mortality rate [1,2]. Because there are no symptoms until late tumor stages, only 20–25% of the diagnosed cases are operable. Moreover, there is no effective diagnostic biomarkers or therapeutic agents. Consequently, the prognosis is very poor [3]. Therefore, development of novel therapeutic agent is urgently needed. Currently, gemcitabine and 5-FU are two common therapeutic agents used [4–6] and combinatory therapies show some progress [7].

The LINCS (Integrated Network-Based Cellular Signature) is a NIH funded program that has been collected expression profiles concerning (showing) how human cells respond to chemical, genetic, and disease perturbations. The LINCS program is implemented in two steps. Phase 1 focused on the initial production of perturbation-induced molecular, cellular signature, and assay development. Phase 2 focuses on high-throughput experiments starting in 2014 to investigate changes that occur when other cell lines are exposed to perturbation. The purpose of the LINCS program is to understand human disease and develop new therapies [8]. L1000CDS^2 is a LINCS L1000 signature search engine that lists small molecules that are predicted to promote or reverse the input signatures. Considering cancer is a genetic disease, finding a "perturvant" that restores aberrant expression changes induced by genetic alterations is a reasonable and suitable way for personalized therapy [9–11].

Drug repositioning is the application of existing drugs or compounds to treat other diseases. The drug has been approved for other uses, has not been withdrawn due to side effects, or has not been approved for

* Corresponding author.
** corresponding author
E-mail addresses: singhshr@mail.nih.gov (S.R. Singh), drksc@amc.seoul.kr (S.C. Kim), suhwan.chang@amc.seoul.kr (S. Chang).

https://doi.org/10.1016/j.canlet.2019.08.002
Received 14 May 2019; Received in revised form 7 August 2019; Accepted 7 August 2019
0304-3835/ Published by Elsevier B.V.

efficacy [12,13]. There was an example of successful drug repositioning using the Met-express algorithm [14] in lung, liver and breast cancer [15]. In pancreatic cancer, the key enzyme-coding gene in cancer metabolism was predicted using the Met-express algorithm, and the candidate drug was selected having expression in the C-map and drug-induced gene rank list using key pancreatic cancer enzyme [2].

BX-795 was identified as a 3-phophoinositidie-dependent protein kinase 1 (PDK1) inhibitor with potent activity in blocking PDK1/AKT/mTOR signaling [16–18]. BX-795 also inhibits the TANK-binding protein 1 (TBK1) and IκB kinase ε (IKKε), which in turn inhibit the phosphorylation, nuclear translocation and transcriptional activity of interferon regulatory factor 3 (IRF3) [17,19]. In human oral squamous cell carcinoma, BX-795 shows antitumor activity through apoptosis [19]. Also, in bladder cancer, BX-795 inhibits the proliferation and migration [20].

In this study, we presented a bioinformatic approach to select drug candidate for PDAC using GEO database and L1000CDS^2 tool. Among the six candidates screened by this approach, we further demonstrate BX-795 effectively suppress PDAC growth in vitro and vivo.

2. Materials and methods

2.1. Microarray data acquisition

Microarray dataset was obtained from the Gene Expression Omnibus (GEO, http://www.ncbi.nlm.nih.gov/geo) shown in Table 1. In order to identify genes that are abnormally expressed in pancreatic cancer, we used a web tool GEO2R, that produces top 250 up-regulated genes from each of the PDAC expression set listed below. We performed L1000CDS^2 analyses using the gene list as a input, to find agent that reverses the up-regulated genes in PDAC (http://amp.pharm.mssm.edu/L1000CDS2/#/index).

2.2. Cell culture

Pancreatic primary cancer cell was cultured in RPMI with 5% FBS, 1% penicillin/streptomycin, 20 ng/ml EGF, 4 μg/ml hydrocortisone and 4 μg/ml transferrin. HPDE (Human pancreatic duct epithelial) cells were cultured in keratinocyte serum-free medium supplemented with EGF and bovine pituitary extract. All cells were cultured at 37 °C with 5% CO_2.

2.3. Proliferation assay

Cells were seeded in a 96 well plate at a density of 3000 cells/well in 50 μl culture media. After 24hrs of seeding, drug was treated onto cells. To monitor cell proliferation, 1/10 volume of AlamarBlue, or EZcytox was added directly to cells after 72hrs of the drug treatment. The cells were incubated for 2 h before measuring viability, which was detected by a microplate fluorescence spectrophotometer (SpectraMax340pc384, Molecular Devices).

2.4. Determination of IC_{50} values

In order to calculated IC_{50} value, each drug was diluted in 10-fold for 4 points. The cell viability was defined as (mean BX-795, LDN-193189, CGP-60474, Narciclasine, Importazole, AT-7519-treated A_{450} - blank)/(mean untreated control A_{450} – blank) x 100. The IC_{50} values were determined by Graphaped Prism software.

2.5. RNA preparation and real time PCR

RNA extraction was performed using Tri-RNA (FAVOGEN). 1 μg of the RNA was used for cDNA synthesis (Takara) according to the manufacturer's instructions. Real-time PCR was performed with SYBR Green in a Bio-Rad real-time PCR detection system. The primers used for qRT-PCR were as follows:

PDK1, 5′-CCTCTGGCTGGTTTTCCTTA-3′ and 5′-CGTGGTTGGTGGTTGTAATGC-3’; TBK1, 5′-CCTCCCTAAAGTACATCCACG-3′ and 5′-CAATCAGCCATCGTATCCCC-3’’.

RhoA, 5′-TTCCATCGACAGCCCTGATAGTTTA-3′ and 5′-CACGTTGGGACAGAAATGCTTGR-3’.

CDK1, 5′-GGGGATTGTGTTTTGTCACTC-3′ and 5′-AGGCTTCCTGGTTTCCATTT-3’; BMPR1A, 5′-CAGGTTCCTGGACTCAGCTC-3′ and 5′-TGGTATTCAAGGGCACATCA-3’

Table 1
The main features of 10 selected GEO dataset for PDAC.

Datasets	Platform	Samples in total	Submission data	Citation(s) on
GSE15471	GPL570	78	Mar 31, 2009	Hepatogastroenterology 2008 Nov–Dec; 55(88):2016-27. PMID: 19260470
GSE16515	GPL570	52	Jun 09, 2009	Cancer Cell 2009 Sep 8; 16(3):259-66. PMID: 19732725
GSE28735	GPL6244	90	Apr 20, 2011	PLoS On e2012; 7(2):e31507. PMID: 22363658, Clin Cancer Res 2013 Sep 15; 19(18):4983-93. PMID: 23918603
GSE46234	GPL570	8	Apr 19, 2013	–
GSE55643	GPL6480	53	Mar 06, 2014	Oncotarget 2014 Nov 30; 5(22):11064-80. PMID: 25415223
GSE60980	GPL14550 GPL15159	182	Sep 02, 2014	Mol Oncol 2015 Apr; 9(4):758-71. PMID: 25579086
GSE62165	GPL13667	131	Oct 08, 2014	BMC Cancer 2016 Aug 12; 16:632. PMID: 27520560
GSE62452	GPL6244	130	Oct 17, 2014	Cancer Res 2016 Jul 1; 76(13):3838-50. PMID: 27197190
GSE71989	GPL570	22	Aug 12, 2015	–
GSE91035	GPL22763	50	Dec 08, 2016	–

2.6. Protein extraction and western blotting

Cells were harvested and lysed in radioimmunoprecipitation assay (RIPA) buffer containing protease inhibitors. After centrifugation at 14,000 rpm for 15min, the supernatant was collected, and the protein concentration was determined by BCA assay. Protein samples were separated on SDS-PAGE, transferred to a PVDF membrane. Immunoblotting was performed with antibodies against TBK1(Cell signaling Technology), p-TBK1(Ser172) (Cell signaling Technology), PDK1(Cell signaling Technology), p-PDK1(Ser241) (Cell signaling Technology), AKT(Cell signaling Technology), p-AKT(Ser473) (Cell signaling Technology), p-AKT(Thr308) (Cell signaling Technology), p-mTOR(Ser2448) (Cell signaling Technology), p-GSK3β(Ser9) (Cell signaling Technology), p-S6K(Thr389) (Cell signaling Technology), MEK (Cell signaling Technology), p-MEK(Cell signaling Technology), ERK (Cell signaling Technology), p-ERK(Cell signaling Technology), PARP (Cell signaling Technology), caspase-7(Cell signaling Technology), E-cadherin (Cell signaling Technology), Slug(Cell signaling Technology), Vimentin(Cell signaling Technology), Snail(Cell signaling Technology), Twist(Cell signaling Technology) and β-actin(Santa Cruz Biotechnology).

2.7. Migration assay

Cell mobility was measured using transwell chambers with 6.5-mm diameter polycarbonate filters (8.0 μm pore size). In brief, cells were resuspended at a final concentration of 1×10^5 cell/ml, in serum free medium. One hundred microliters of the cell's suspension were loaded into each of the upper wells. 10% FBS were used as chemo-attractants in the lower chambers, and the chamber was incubated at 37 °C for 24 h. The cells were fixed and stained with hematoxylin and eosin. Non-migrated cells on the upper surface of the filter were removed by wiping with a cotton swab, and migration ability was measured by counting cells that had migrated to the lower side of the filter, using an optical microscope.

2.8. Animal experiments

The animal experiments were performed in accordance with the Korean Ministry of Food and Drug Safety (KMFDS) guidelines. Protocols for animal experiment were reviewed and approved by the Institutional Animal Care and Use Committees (IACUC) of Asan Institute for Life Sciences (AILS, Project Number: 2015-12-164). All mice were maintained in the specific pathogen–free (SPF) facility of the Laboratory of Animal Research in the Asan Medical Center. For xenograft, pancreatic cancer primary cells were harvested, and resuspended at 5×10^6 cells/100 μl in matrigel and PBS. Then, 5×10^6 cells/100 μl were injected into male BALB/c nude mice. When the tumor volume was approximately 100 mm^3, the treatment was started in five groups: control, gemcitabine, BX-795 and BX-795 plus trametinib combination. BX-795 and gemcitabine were administered twice a week for three weeks, and trametinib was administered five times a week for three weeks. The drugs were delivered by i.p. injection and oral administration with BX-795 (25 mg/kg), gemcitabine (25 mg/kg) and trametinib (1 mg/kg). Tumors were measured using calipers, and tumor volume was calculated as follows: Tumor volume (mm^3) = L X W^2 ÷ 2. Tumor volume and mouse body weight were measured twice a week.

2.9. Immunohistochemistry

The tumors were fixed in 10% formalin and embedded in paraffin. Paraffin-embedded blocks were sectioned 5 μm slices. The TUNEL assay was performed using an in-situ Apoptosis Detection Kit (Takara) according to the instructions of the manufacturer. The Ki-67 staining of the tumor tissue samples was performed by using the auto-immunostainer BENCHMARK XT (VENTANA MEDICAL SYSTEMS, TUCSON, AZ, USA) with OPTIVIEW DAB DETECTION KIT (VENTANA MEDICAL SYSTEMS, TUCSON, AZ, USA) according to the manufacturer's instructions and using the reagents supplied with the kit. Immunohistochemistry was performed with antibodies to MOUSE anti-Ki-67 (cat. M7240, clone MIB1, dilution 1:300, DAKO, DENMARK, GLOSTRUP). For each group of n = 3, counting was performed on each of the four pictures to obtain the average value, and then the average value from one group.

2.10. Statistical analysis

Statistical analysis was performed with GraphPad Prism 5 using the Student's t-test.

3. Results

3.1. Identification of "perturvants" that reverses abnormal PDAC gene alteration, via GEO2R data analysis and L1000CDS^2 webtool

To obtain input data for *L1000CDS^2* search tool, we selected 10 microarray datasets (GSE 15471, 16515, 28735, 46234, 55643, 60980,

Table 2
20 drug candidates obtained from L1000CDS^2 analysis of 10 PDAC expression datasets.

Rank	Perturbation	Average rank[a]	Number of counting
1	Homoharringtonine	5	2
2	BX-795	7.25	4
3	PAC 1	13.5	3
4	PERHEXILINE MALEATE	14	2
5	TG101348 (Fedratinib)	14.5	2
6	Ingenol 3, 20-dibenzoate (IBD)	15	9
7	BRD-K91145395 (Prostratin)	17.1	14
8	Narciclasine	20.6	3
9	BRD-A46747628 (Ouabain)	23	1
10	DG-041	23.5	2
11	JAK3 Inhibitor VI	26	2
12	Importazole	26.2	5
13	IMD 0354	26.5	2
14	PLX-4720	26.6	5
15	Emetine Dihydrochloride Hydrate (74) (EMETINE)	27.25	4
16	QS 11	27.5	2
17	CGP-60474	30	9
18	Mevastatin (Compactin)	30	3
19	LDN-193189	30.5	2
20	AT-7519	59.6	3

[a] The value of average rank is the sum of the perturbation rank from each dataset, divided by the number of datasets with the drug predicted.

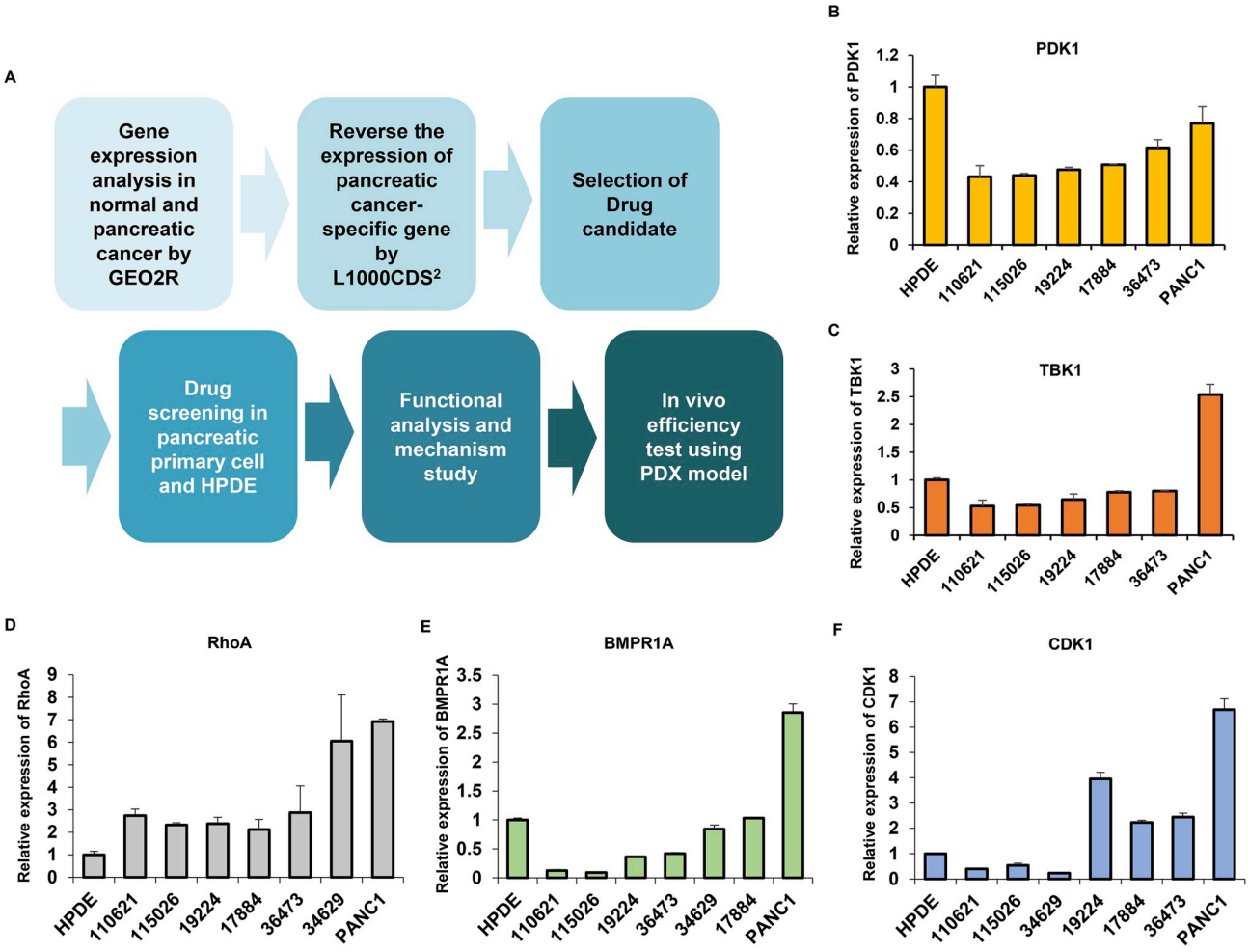

Fig. 1. Identification drug candidates for PDAC using GEO dataset and L1000CDS tool (A) The overall scheme of the virtual screening and validation. Gene expression data from GEO was used as input data for L1000CDS pharmacogenetic search tool. The candidates are further tested in patient-derived cells and xenograft model (B–F). The expression levels of PDK1 and TBK1 (target genes of BX-795; B and C), RhoA (target gene of Narciclasine; D), BMPR1A (target gene of LDN-193189; E), and CDK1 (target gene of CGP-60474 and AT-7519; F) in pancreatic cancer primary cells, pancreatic cancer cell line and HPDE (Human pancreatic duct epithelial cell).

62165, 62452, 71989, 91035) of PDAC from GEO database (See methods for detail). Each dataset was analyzed with GEO2R, to obtain fold change of gene expression between normal and tumor samples. We selected genes that are higher/lower in tumor more than two folds compared to normal control (Supplementary Table 1). The list of selected genes was entered to the L1000CDS^2 webtool to search for substances that can reverse the expression changes (referred as perturvants). As an output, top 50 perturvants were identified from each GEO dataset (Supplementary Tables 2–11). Table 2 shows a summarized list of 20 agents that appeared most frequently and showed high probability as a perturvant. Among them, we selected 6 drugs including BX-795, CGP-60474, LDN-193189, Narciclasine, Importazole and AT-7519. We did not include Prostratin even though it appeared most frequently and had a high probability as a perturvant. This is because it has been previously studied for pancreatic cancer [21]. The overall scheme of the screening is summarized in Fig. 1A. The expression of target genes for the six selected agents are shown in Fig. 1B–F.

3.2. Selection of BX-795 as a potential anti-PDAC drug

In order to validate the predictability of L1000CDS^2 webtool, we examined the anti-proliferative effect of the six compounds in four pancreatic primary cancer cells [21], along with normal pancreatic ductal epithelial cell HPDE (Fig. 2). The IC_{50} value for the six compounds were summarized in Table 3. The IC_{50} of Narciclasine was low for all the PDAC cells (from 0.003 to 0.049 μM). However, it was also

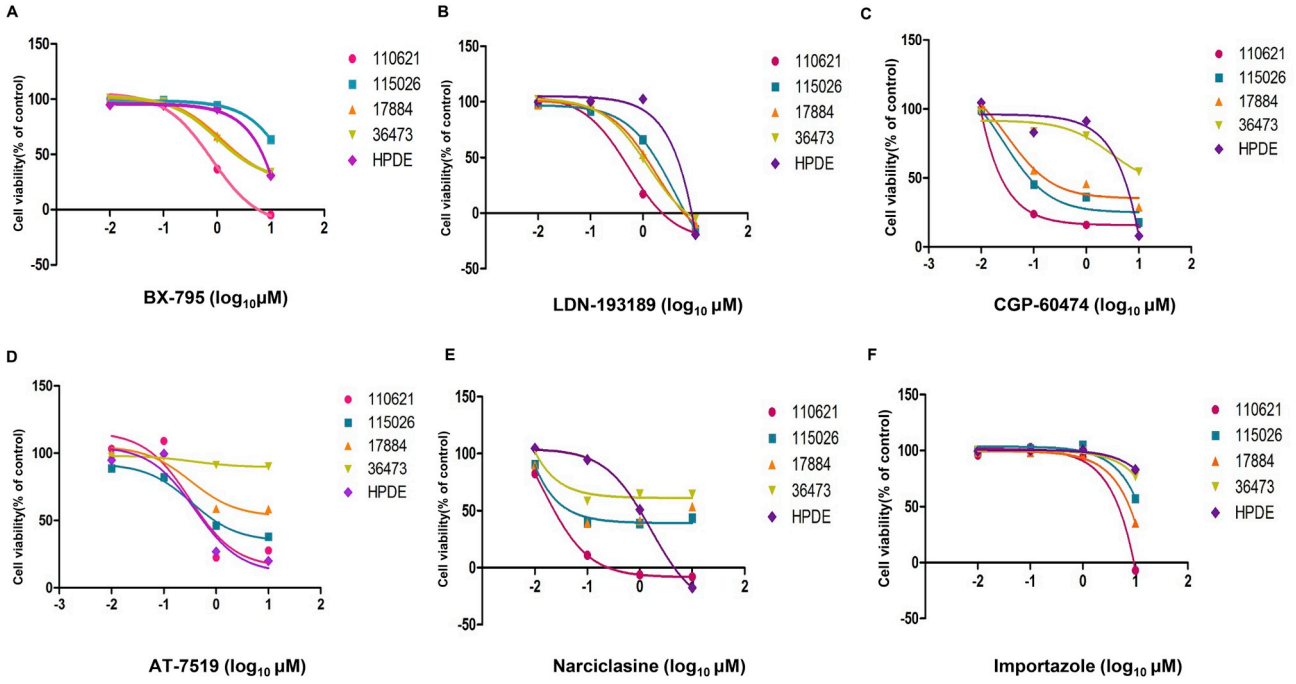

Fig. 2. Determination of IC_{50} curves of the six drug candidates for PDAC. (A–F) Graphs show cell viability after the treatment with BX-795 (A), LDN-193189 (B), CGP-60474 (C), AT-7519 (D), Narciclasine (E) and Importazole (F) in pancreatic cancer primary cells (110621, 115026, 17884 and 36473) and HPDE (Normal cell control, purple line). (For interpretation of the references to colour in this figure legend, the reader is referred to the Web version of this article.)

Table 3
IC_{50} values of selected six drug candidates.

Cells Tested	Repeat	BX-795	LDN-193189	CGP-60474	AT-7519	Narciclasine	Importazole
110621	1	0.7956	0.5411	0.01874	0.3192	0.01423	N/A
	2	0.8639	0.5499	0.03564	0.2712	0.01548	N/A
115026	1	56.54	3.995	0.02720	0.3385	0.00381	N/A
	2	46.58	5.296	0.03962	0.4006	0.00709	N/A
17884	1	1.223	1.744	0.03186	0.3301	0.0104	N/A
	2	1.535	1.112	0.01143	0.324	0.049	N/A
36473	1	0.9850	1.243	N/A	N/A	N/A	N/A
HPDE	1	4.484	9.636	2.388	0.3939	0.05688	N/A
	2	3.166	2.832	1.014	0.5774	0.02819	N/A

low for HPDE suggesting the drug is toxic to normal cells as well. similarly, the IC_{50} values of AT-7519 were approximately 0.3 μM in all cells tested, suggesting these compounds are cytotoxic to both of cancer and normal cells. Therefore, we excluded Narciclasine and AT-7519 for further study. Also, we found Importazole was not effective showing IC_{50} more than 10 μM, and LDN-193189 was already studied in pancreatic cancer [22]. Therefore, we focused on BX-795 for further analysis.

3.3. BX-795 inhibits mTOR-GSK3β signaling and increases apoptosis

BX-795 is known to inhibit PDK1 and TBK1 [16–18]. and our real-time PCR results showed comparable RNA level of the two targets among 4 primary cells tested (Fig. 1B and 1C). Thus, the four pancreatic primary cancer cells, and HPDE (human pancreatic duct epithelial cell) were tested for the anti-proliferative effect of BX-795. After 72 h, the IC_{50} values of BX-795 were approximately 4.4, 0.8, 1.2, 0.9 and 50 μM

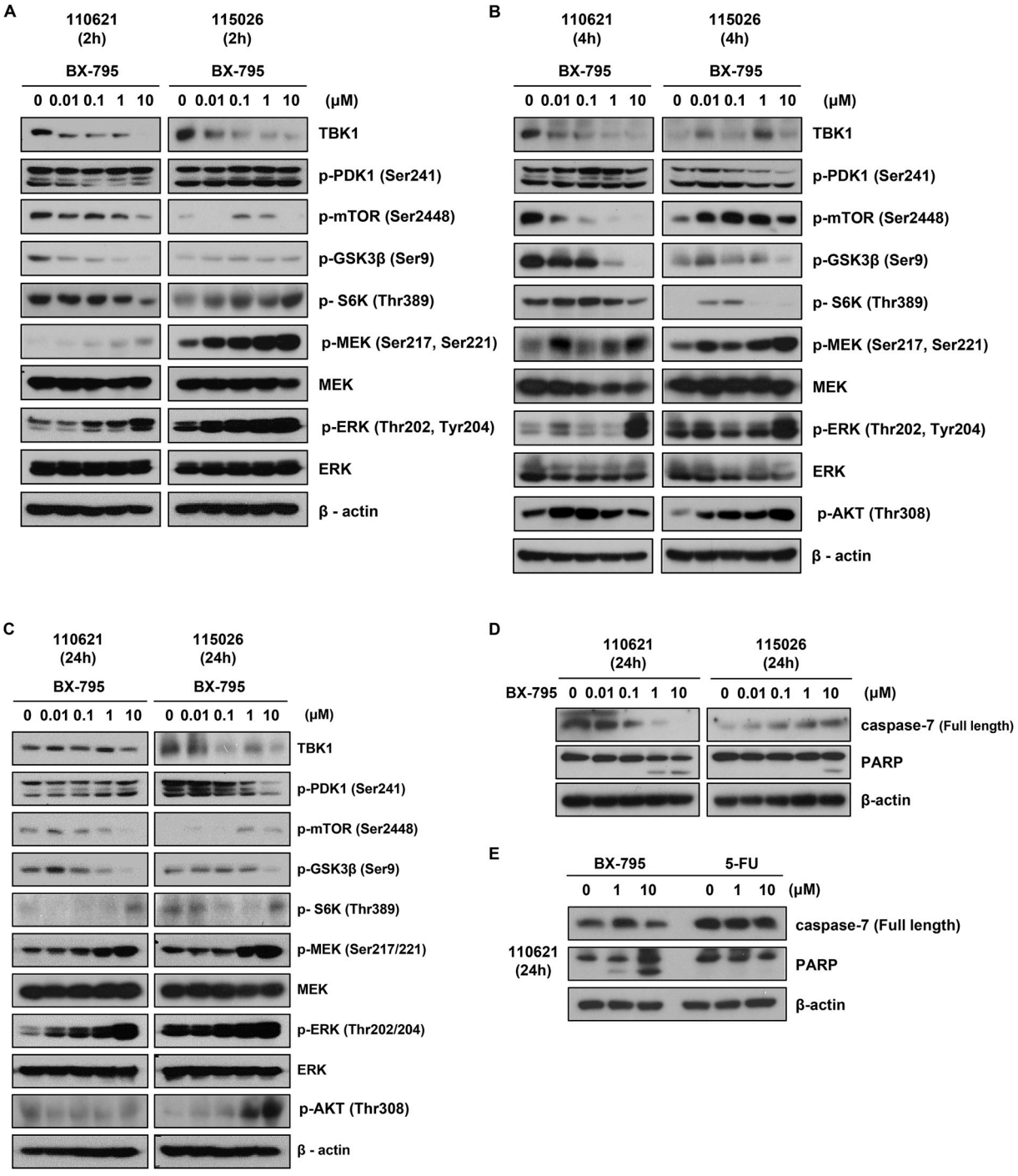

Fig. 3. BX-795 inhibits mTOR-GSK3β signaling and trigger apoptosis in primary pancreatic cancer cells. (A–C) Western blot analysis for TBK1, p-PDK1(Ser241), p-mTOR(Ser2448), p-GSK3β(Ser9), p-MEK(Ser217, Ser221), p-ERK(Thr202, Tyr204) and p-AKT(Thr308). Two pancreatic primary cancer cells, 110621 and 115026, were treated with increasing dose of BX-795 for 2 h s(A), 4 h s (B) and 24 h s(C). (D, E) Western blot analysis for apoptosis markers in two pancreatic primary cancer cells (110621, 115026) after treatment with BX-795 or 5-FU. Note that the decreased Caspase-7 (full length) and cleaved PARP (Smaller band) indicate apoptosis.

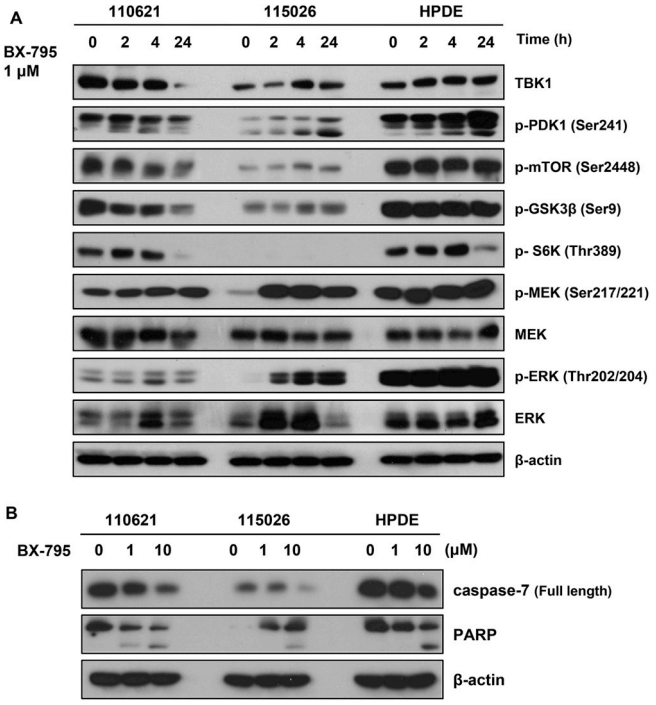

Fig. 4. BX-795 is more effective in primary pancreatic cancer cells than normal cells.
(A) Western blot analysis of pancreatic primary cancer cells (110621 and 115026) and HPDE (normal control) for TBK1, p-PDK1(Ser241), p-mTOR (Ser2448), p-GSK3β(Ser9). The concentration of BX-795 was fixed at 1 μM and incubated for 2 h s, 4 h s and 24 h s. (B) Comparative analysis for Caspase-7 and PARP cleavage in two primary cancer cells and HPDE. Increasing dose of BX-795 were treated for 24 h. Note the 110621 cells show more PARP cleavage than HPDE, in lower dose of BX-795.

for HPDE, 110621, 17884, 36473 and 115026, respectively (Table 3). Interestingly, Western blot analysis showed both 110621 and 115026 cells have high level of p-PDK1 (Supplementary Fig. 1). In contrast, the IC_{50} value of BX-795 in 115026 was 50 times higher than 110621 (Table 3), suggesting a resistant mechanism exists in 115026 cells. Therefore, we treated these two cells with increasing doses BX-795 and monitored its downstream signaling pathway (mainly AKT-mTOR and GSK3β-MEK) by western blotting. After 2 h of BX-795 treatment, we observed p-mTOR(Ser2448) and p-GSK3β(Ser9) were decreased in 110621. In 115026, however, we could not find such changes, implying these responses to BX-795 cause difference in the drug sensitivity. Interestingly, we found increased p-MEK and p-ERK in both cells with more dramatic increase in 115026 cells (Fig. 3A), suggesting the mechanism of resistance to BX-795 mediated by MEK-ERK pathway. When we repeated the same analysis after 4 h or 24hrs of BX-795 treatment, we found consistently decreased level of p-mTOR (Ser2448) and p-GSK3β(Ser9) in 110621 whereas In 115026, up-regulated p-mTOR (Ser2448) and marginally decreased p-GSK3β(Ser9) were observed (Fig. 3B and 3C). Consequently, we observed decreased Caspase-7 level and increased PARP cleavage in 110621 cells on lower dose of BX-795 (Fig. 3D), indicating that 110621 cells undergo more apoptosis than 115026 upon BX-795 treatment. The change of apoptotic markers by BX-795 on 110621 PDAC cell was more evident than the treatment of 5-FU, a standard drug for PDAC treatment (Fig. 3E).

3.4. BX-795 shows better anti-proliferative effect in PDAC cells than normal cells

Next, we examined the effect of BX-795 in normal HPDE cells that showed about 5 times higher IC_{50} value than 110621 cells (Table 3). The concentration of BX-795 was fixed to 1 μM in 110621, 115026 and HPDE cells with varying time points of 0, 2, 4 and 24 h. The results in Fig. 4A shows p-GSK3β(Ser9) and p-mTOR(Ser2448) were decreased in 110621 whereas HPDE cells showed high, unchanged level of p-GSK3β(Ser9), p-mTOR(Ser2448) and marginal increase of p-ERK. The quantitation of the protein level by densitometry is shown in Supplementary Fig. 2, confirming 110621 cells is more sensitive to BX-795 treatment. Consistently, when compared to 110621 cells, we found the HPDE cells are less apoptotic in response to BX-795 (Fig. 4B). Moreover, by treating another primary cancer cell (17884) with the BX-795, we confirmed BX-795 causes comparable pattern of p-GSK3β(Ser9) reduction and increased p-ERK in other PDAC cells (Supplementary Fig. 3A). We also found the p-AKT level in HPDE cell was marginally affected by BX-795 (Supplementary Fig. 3B), consistent with the data in Fig. 4A.

3.5. Inhibition of PDAC cell migration by BX-795

On the way of BX-795 treatment, we noticed marked morphological change of PDAC and HPDE cells (Supplementary Fig. 4). Hence, we examined if the BX-795 can affect cellular migration by transwell assay. As shown in Fig. 5A–D, the treatments of BX-795 on 110621 and 115026 showed a significant decrease in migration. When compared to 5-FU (Fluorouracil), BX-795 showed comparable anti-migratory effect with mild degree of anti-proliferative effect (Supplementary Fig. 5A -5C). Molecularly, when we checked the EMT markers, we found the expression of Slug and Snail were decreased in 110621 whereas the expression of Vimentin and Slug were decreased in 115026 (Fig. 5E). For Vimentin and Snail, which were not detected by Western blot in either 110621 or 115026 cells, mRNA level was analyzed. The data in Fig. 5F indicates Snail expression is significantly decreased in 115026 cells by BX-795 treatment. We also found the p-AKT level in HPDE cell was marginally affected by BX-795 (Supplementary Fig. 3B), consistent with the data in Fig. 4A.

3.6. Additive antitumor effect of BX-795 in combination with trametinib

Even though BX-795 showed expected antitumor effect in PDAC cells, the up-regulated p-MEK by BX-795 is unexpected. The increase was dose-dependent and more dramatic in 115026 at 2–4 h s after treatment (Fig. 3A and 3B). Therefore, we questioned if the

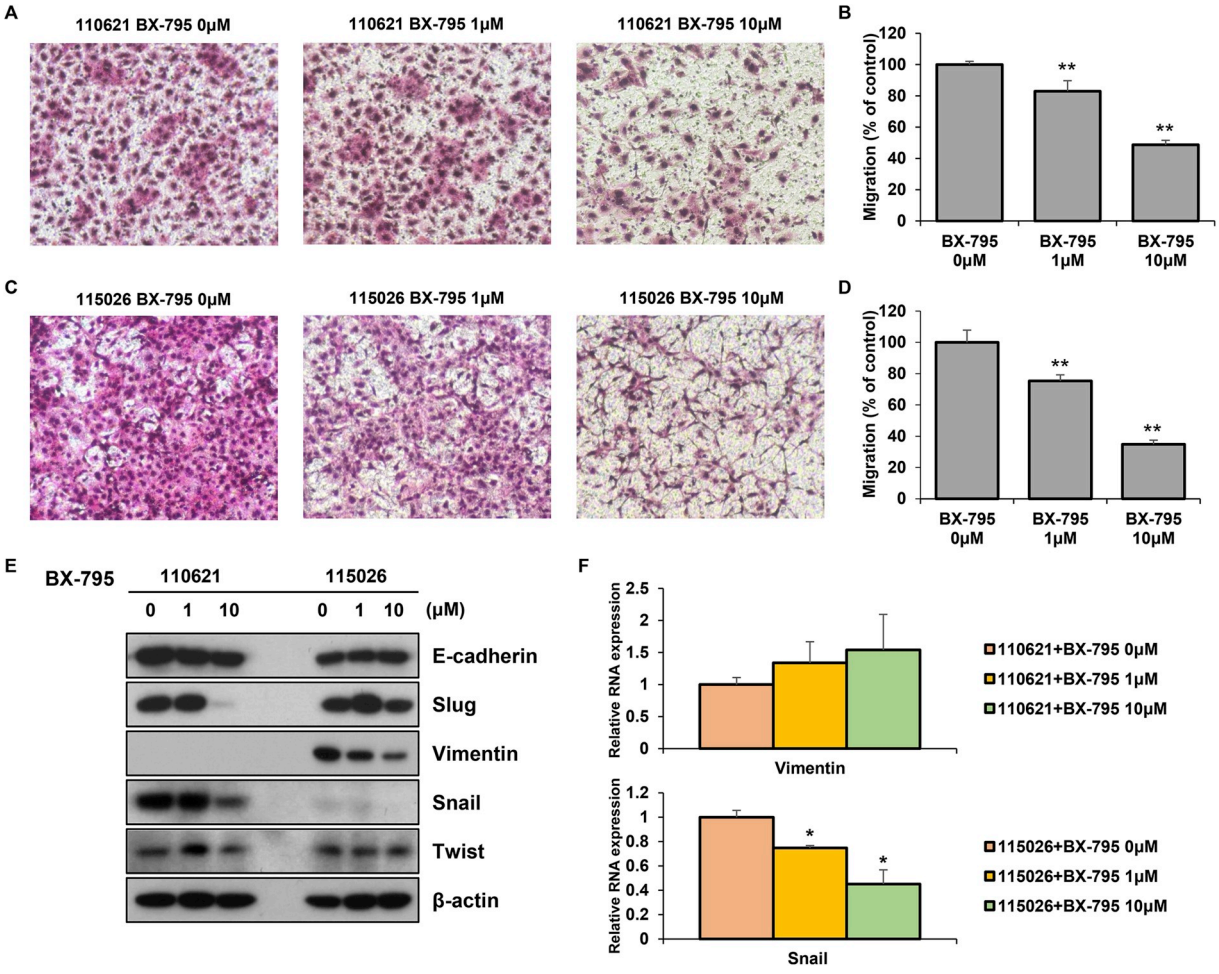

Fig. 5. BX-795 inhibits the migration of pancreatic primary cancer cells.
(A–
D) Results of cell migration measured by transwell assay in 110621 (A and B) or 115026 (C and D) cells. A and C are representative images of migrated cells in response to increasing BX-795. B and D are quantitation of the results A and C respectively (E) Western blot analysis of EMT markers in the 110621 and 115026 cells, indicating reduced Slug or Snail expression (F) Real-time RT-PCR quantitation of two EMT markers that were not clear by W
estern blot analysis. (*P $<$ 0.05, **P $<$ 0.01).

combinatory treatment of BX-795 with MEK inhibitor (trametinib) can overcome the resistance of 115026 and sensitize 110621 cells upon BX-795. As expected, the treatment of trametinib resulted in efficient inhibition of ERK (Fig. 6C and 6D). However, we could not observe inhibitory effect of trametinib on 115026 cells (see discussion). Instead, we found the combination of BX-795 and trametinib reduced cell proliferation in 110621, with an efficient p-ERK inhibition when trametinib 1 nM are treated with 1 μM of BX-795 (Fig. 6A and 6B). These data suggest 115026 PDC might have other mechanism of BX-795 resistance but 110621 cells are dependent on MEK-ERK pathway to survive. Based on the results in Fig. 5, we also tested the three EMT markers after BX-795 + trametinib. We observed similar effect on the levels of Snail with Trametinib alone or Trametinib BX-795 combination, which suggest that suppression of EMT may not be the only mechanism for enhanced efficacy of the combination compared to Trametinib alone (Fig. 6E). In addition, we also examined the effect of combination of BX-795 plus clinically used PDAC drugs. We found Gemcitabine (a standard therapeutic agent for PDAC) was not able to synergistically inhibit PDAC cell growth in combination with BX-795 (Supplementary Figs. 6A and 6C, even though p-S6K or p-GSK-3b was decreased (Supplementary Figs. 6B and 6D). In contrast, we found 5-FU show significant growth inhibition in combination with BX-795, for both PDAC cells (Supplementary Fig. 7).

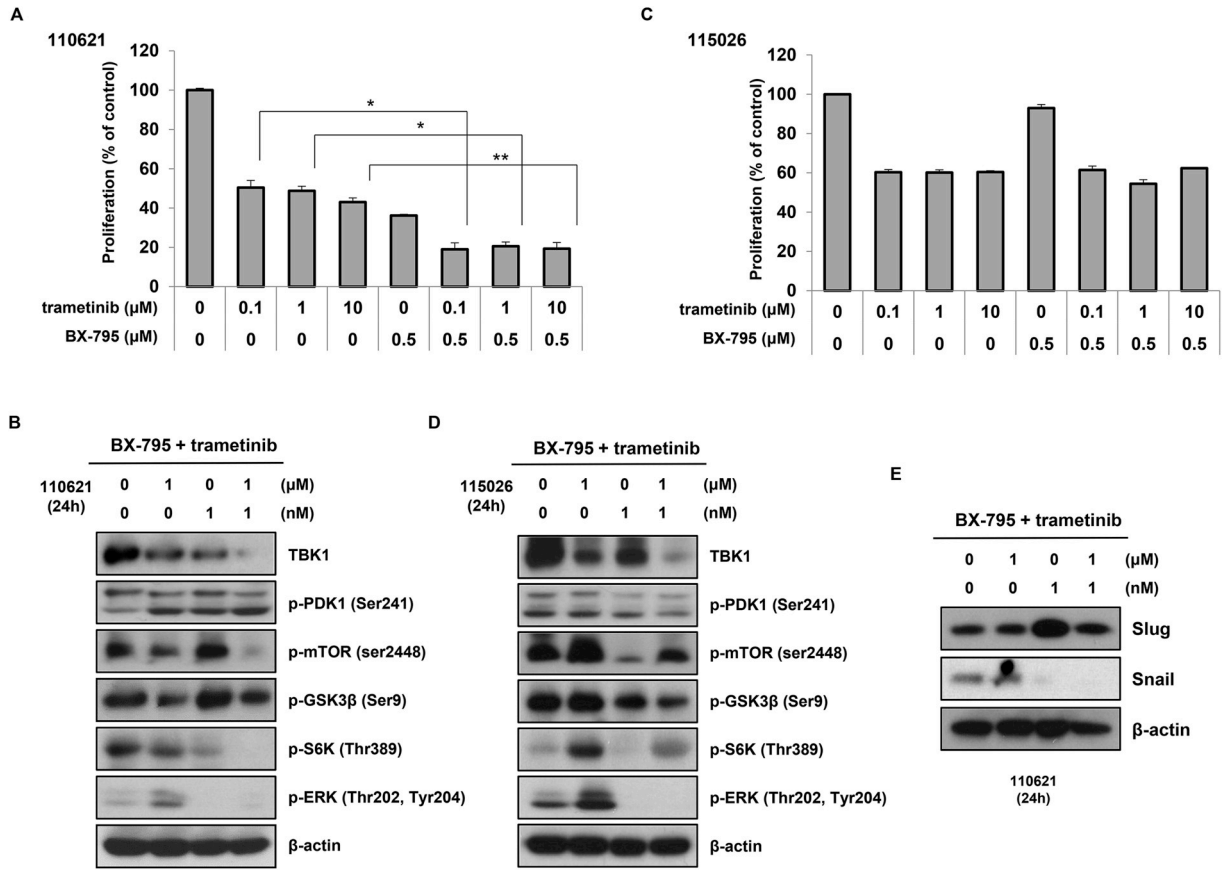

Fig. 6. The combination of BX-795 and MEK inhibitor (Trametinib) inhibits the proliferation of 110621 primary cells. (A) Graph showing the proliferation of 110621 cells after the treatment of BX-795 (0, 0.5 μM) combined with trametinib (0, 0.1, 1, 10 μM). (B) Western blot analysis of TBK1, p-PDK1(Ser241), p-GSK3β(Ser9) and p-ERK(Thr202, Tyr204) in 110621 cells after the treatment of BX-795 (0, 1 μM) in combination with trametinib (0, 1 nM). (C, D) The same analysis as shown in (A) and (B) were done for 115026 cells. (*P < 0.05, **P < 0.01) (E) Western blot of two EMT markers (Slug and Snail) after the combination of BX-795 plus trametinib on 110621 cells.

3.7. BX-795 inhibits PDAC tumor growth in vivo

Based on the findings shown above, we proceed to examine the in vivo efficacy of BX-795. We also questioned if the combination of trametinib (MEK inhibitor) with BX-795 can exert synergistic or additive antitumor effect in 110621 PDX. As shown in Fig. 7A, when the tumor volume was measured after each of the drug treatment, we found BX-795 efficiently inhibit tumor growth by itself (yellow line), comparable to the gemcitabine (orange line). The tumor volume at the end point supported this result as well (Fig. 7B). In addition, when we combined BX-795 with the MEK inhibitor trametinib, we could see a significant reduction of tumor growth compared to BX-795 alone (Fig. 7A, pink line). This result is consistent with the in vitro results that showed increased growth inhibitory effect when BX-795 and trametinib were combined (Fig. 6A). We further analyzed PDX tumors by IHC, with TUNEL and Ki-67 that are apoptosis and proliferation marker, respectively (Supplementary Fig. 6 for raw data). Representative IHC images are shown in Fig. 7C. Counting of TUNEL positive cells for each group of tumors revealed treatment with BX-795 or its combination with trametinib show more apoptotic cells than tumor treated with gemcitabine, while there were few apoptosis cells present in the control group (Fig. 7D). Conversely, we found the lowest number of Ki-67-positive cells from tumors treated with BX-795 plus Trametinib, whereas BX-795 single treatment showed similar Ki-67 positive cells to gemcitabine treated tumor (Fig. 7E). Altogether, these results demonstrate BX-795 suppresses PDAC growth in vivo and combination with Trametinib enhances the antitumor effect.

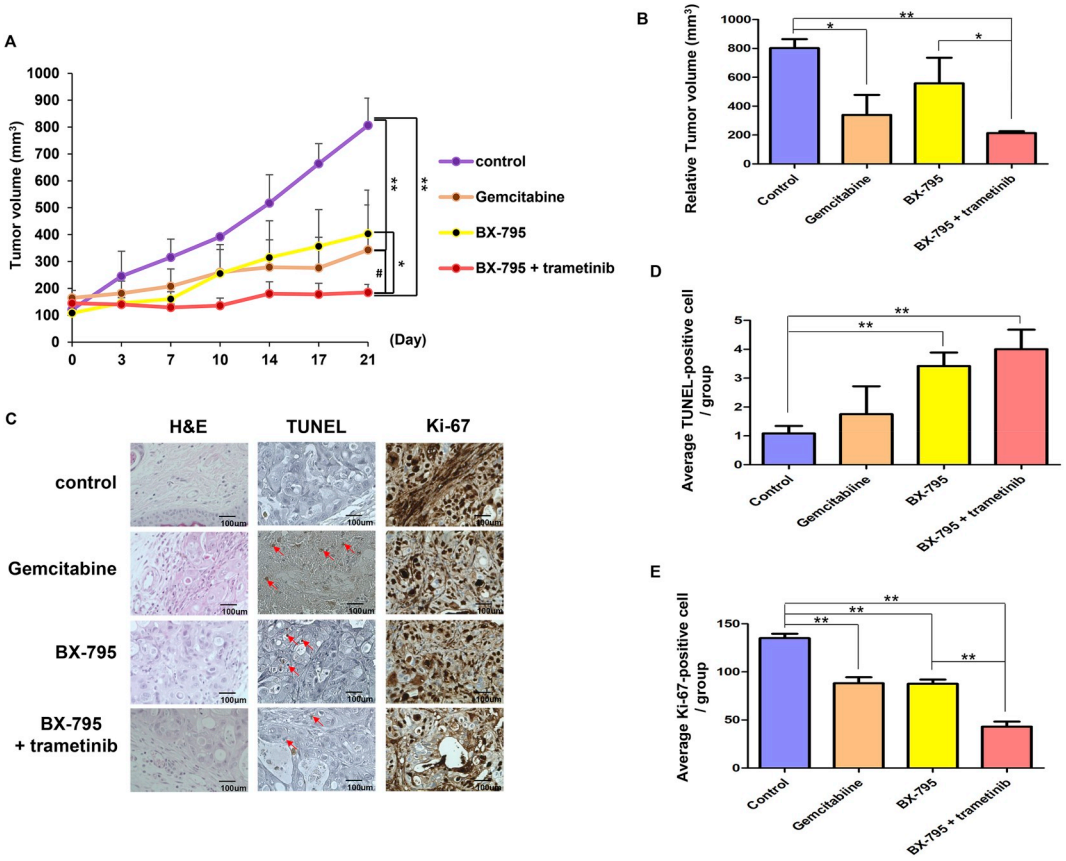

Fig. 7. In vivo antitumor effect of BX-795 in the pancreatic patient-derived xenograft model. (A) A graph showing the tumor volume measured during the treatment. BX-795, Gemcitabine or trametinib was administered as monotherapy or in combination, and tumor growth was monitored (n = 4 per group) for three weeks (See Supplementary Table 12 for detailed statistical values). (B) A graph showing the average volume of the tumor at the endpoint. (C) Representative pictures of H&E, TUNEL and Ki-67 staining of control and the three treatment groups: Gemcitabine, BX-795 and combination of BX-795 with trametinib. Red arrows in TUNEL images indicate signal positive cells. (D and E) Graph showing average count of TUNEL-positive (D) or Ki-67 positive (E) cells from each treatment group. Four random area of the stained tumor sections were pictured and analyzed for each tumor sample. *$p < 0.05$, **$p < 0.01$, # = 0.066.. (For interpretation of the references to colour in this figure legend, the reader is referred to the Web version of this article.)

4. Discussion

Our research proposed an efficient, easy bioinformatic process to identify drug candidates for PDAC. The limitation of this approach includes the lack of clinical parameters for expression data that could subgroup each GSE dataset and identify more precise candidate drugs. Despite of that, the combined use of GEO2R and L1000CDS^2 search tool is applicable to all kinds of cancer if the expression profiles are available in GEO database. In our study, we combined 10 GEO dataset of PDAC and obtained 6 chemical "perturvants" that might reverse the abnormal expression changes. Another approach might be producing expression profiles for specific PDCs and use the profile as an "personalized" input data for L1000CDS^2. In this case, however, the lack of appropriate normal control for each of PDC limits its accuracy or applicability. Interestingly, the treatment of 6 compounds on 4 different PDCs showed various sensitivity for each of the PDC against each compound, implying heterogeneity of drug sensitivity in PDAC (Fig. 2). Although we selected and focused on BX-795 for several reasons described above, but we think other candidates are also worthy to be further analyzed. LDN-193189 is a BMP (Bone Morphogenic Protein) pathway inhibitor, targeting ALK1-4 that are receptors of BMP ligand [23]. CGP-60474 is a potent cell cycle dependent kinase (CDK) inhibitor [24] and recently reported as anti-endotoxemic agent [25]. Similarly, AT-7519 is a multi-CDK inhibitor for CDK1, 2, 4, 6 and 9 with IC50 of 10–210 nM [26]. On the other hand, Narciclasine, also known as lycoricidinol, is an isocarbostyril alkaloid found in the Amaryllidaceae (amaryllis) family of flowering plants. It targets elongation factor eEF1A [27] and recently, skeletal muscle [28]. Lastly, importazole (2,4-diaminoquinazoline) is known to specifically blocks importin-β-mediated nuclear import [29].

After the treatment of PDK1 inhibitor, BX-795, we noticed that p-ERK and p-MEK levels were increased (Fig. 3). In a previous report, the level of p-MEK and p-ERK was increased in a concentration-dependent manner when the PI3K/mTOR inhibitor, NPV-BEZ235, was treated to pancreatic cancer cell line. In this model, the treatment of the MEK inhibitor showed a decrease in proliferation through the suppression of mTORC2 [30]. On the other hand, in mutant NRAS melanoma cells, BX-795 inhibited the growth and combination with MEK inhibitors was shown to enhance apoptosis [31]. We think the activation of MEK-ERK pathway in response to PI3K/mTOR pathway inhibition is a typical resistance mechanism of cancer cells and the combinatory treatment of MEK inhibitor might be a reasonable strategy. However, as we have

seen in 115026 cells (Fig. 6C), it may not effective for all the cases. Initially we expected MEK inhibition can be more effective in 115026 cells, as the activation of ERK which is more dramatic in 115026 cells (Fig. 3D). However, the treatment of trametinib that efficiently blocked ERK phosphorylation (Fig. 6B and 6D) failed to suppress the growth of 115026 cells (Fig. 6C). It is possible that the resistance to trametinib is accomplished by the activation of other MAPK while the sensitivity to Bx-795 is dependent on ERK activation upon the drug treatment.

At present, the exact reason for the various BX-795 sensitivity on PDCs is not clear. Of note, in addition to the growth inhibitory effect, the treatment of BX-795 on pancreatic primary cancer cells and showed reduced migration with decreased EMT marker expression (Fig. 5). Considering the BX-795 is PDK1 inhibitor, this inhibitory effect might be via reduced AKT phosphorylation, as the p-AKT phosphorylates GSK3β and inactive form p-GSK3β (ser9) regulates the slug which in turn reduces E-cadherin to cause EMT [32]. Alternatively, the activated ERK regulates the slug expression [33,34]. Our data showed a reduced Slug and Snail in 110621 cells whereas Vimentin and Slug are affected in 115026 cells, suggesting a diverse molecular effect of BX-795 in different PDAC cells. The other possibility of different resistance to BX-795 might be related to the stemness (often linked with drug resistance) of primary PDAC cells. With this idea, we measured the expression of three CSC markers (Oct-4, Nanog, Sox-2) upon the treatment of BX-795. Surprisingly, the RNA level of all of three markers were increased in both PDAC cells (Supplementary Fig. 9). We speculate this is because non-CSC cells are susceptible to BX-795 so that CSCs are enriched by BX-795. This is supported by the BX-795 resistant 115026 cell results, showing less increase of the three markers. However, the basal level of the three CSC markers in 115026 cells were lower than that of 110621 cells, suggesting the stemness of 115026 cells may not cause its overall resistance. Further study will clarify how the stemness markers are changed by BX-795 in PDAC cells.

Despite of the limited in vitro effect of trametinib, we found significant effect of BX-795 plus trametinib, compared to single treatment of Bx-795 (Fig. 7A and 7C). Considering the trametinib has low toxicity, this result support the basis for the application of Bx-795 combined with trametinib as an alternative option for pancreatic cancer treatment. Therefore, understanding how the activation of MEK-ERK is achieved in the drug treated PDAC cells will be critical to overcome BX-795 resistance.

Conflicts of interest

The authors declare that they have no competing interests.

Acknowledgements

This research was supported by the Basic Science Research Program of the National Research Foundation Korea (NRF), funded by the Ministry of Education (grant number: KNRF-2018016359), a grant from the Korean Health Technology R&D Project, Ministry of Health & Welfare, Republic of Korea (Grant Number: HI14C2640) and a grant from the Asan Institute for Life Sciences (Grant No. 2018-571).

Appendix A. Supplementary data

Supplementary data to this article can be found online at https://doi.org/10.1016/j.canlet.2019.08.002.

References

[1] C. Gungor, B.T. Hofmann, G. Wolters-Eisfeld, M. Bockhorn, Pancreatic cancer, Br. J. Pharmacol. 171 (2014) 849–858.
[2] Y. Ma, J. Hu, N. Zhang, X. Dong, Y. Li, B. Yang, W. Tian, X. Wang, Prediction of candidate drugs for treating pancreatic cancer by using a combined approach, PLoS One 11 (2016) e0149896.
[3] A. Makohon-Moore, C.A. Iacobuzio-Donahue, Pancreatic cancer biology and genetics from an evolutionary perspective, Nat. Rev. Cancer 16 (2016) 553–565.
[4] R. Spadi, F. Brusa, A. Ponzetti, I. Chiappino, N. Birocco, L. Ciuffreda, M.A. Satolli, Current therapeutic strategies for advanced pancreatic cancer: a review for clinicians, World J. Clin. Oncol. 7 (2016) 27–43.
[5] M.S. De La Cruz, A.P. Young, M.T. Ruffin, Diagnosis and management of pancreatic cancer, Am. Fam. Physician 89 (2014) 626–632.
[6] S. Gillen, T. Schuster, C. Meyer Zum Buschenfelde, H. Friess, J. Kleeff, Preoperative/neoadjuvant therapy in pancreatic cancer: a systematic review and meta-analysis of response and resection percentages, PLoS Med. 7 (2010) e1000267.
[7] S. Thibodeau, I.A. Voutsadakis, FOLFIRINOX chemotherapy in metastatic pancreatic cancer: a systematic review and meta-analysis of retrospective and phase II studies, J. Clin. Med. 7 (2018).
[8] A.B. Keenan, S.L. Jenkins, K.M. Jagodnik, S. Koplev, E. He, D. Torre, Z. Wang, A.B. Dohlman, M.C. Silverstein, A. Lachmann, M.V. Kuleshov, A. Ma'ayan, V. Stathias, R. Terryn, D. Cooper, M. Forlin, A. Koleti, D. Vidovic, C. Chung, S.C. Schurer, J. Vasiliauskas, M. Pilarczyk, B. Shamsaei, M. Fazel, Y. Ren, W. Niu, N.A. Clark, S. White, N. Mahi, L. Zhang, M. Kouril, J.F. Reichard, S. Sivaganesan, M. Medvedovic, J. Meller, R.J. Koch, M.R. Birtwistle, R. Iyengar, E.A. Sobie, E.U. Azeloglu, J. Kaye, J. Osterloh, K. Haston, J. Kalra, S. Finkbiener, J. Li, P. Milani, M. Adam, R. Escalante-Chong, K. Sachs, A. Lenail, D. Ramamoorthy, E. Fraenkel, G. Daigle, U. Hussain, A. Coye, J. Rothstein, D. Sareen, L. Ornelas, M. Banuelos, B. Mandefro, R. Ho, C.N. Svendsen, R.G. Lim, J. Stocksdale, M.S. Casale, T.G. Thompson, J. Wu, L.M. Thompson, V. Dardov, V. Venkatraman, A. Matlock, J.E. Van Eyk, J.D. Jaffe, M. Papanastasiou, A. Subramanian, T.R. Golub, S.D. Erickson, M. Fallahi-Sichani, M. Hafner, N.S. Gray, J.R. Lin, C.E. Mills, J.L. Muhlich, M. Niepel, C.E. Shamu, E.H. Williams, D. Wrobel, P.K. Sorger, L.M. Heiser, J.W. Gray, J.E. Korkola, G.B. Mills, M. LaBarge, H.S. Feiler, M.A. Dane, E. Bucher, M. Nederlof, D. Sudar, S. Gross, D.F. Kilburn, R. Smith, K. Devlin, R. Margolis, L. Derr, A. Lee, A. Pillai, The library of integrated network-based cellular signatures NIH program: system-level cataloging of human cells response to perturbations, Cell Syst 6 (2018) 13–24.
[9] Q. Duan, S.P. Reid, N.R. Clark, Z. Wang, N.F. Fernandez, A.D. Rouillard, B. Readhead, S.R. Tritsch, R. Hodos, M. Hafner, M. Niepel, P.K. Sorger, J.T. Dudley, S. Bavari, R.G. Panchal, A. Ma'ayan, L1000CDS(2): LINCS L1000 characteristic direction signatures search engine, NPJ Syst Biol Appl 2 (2016).
[10] B. Chen, L. Ma, H. Paik, M. Sirota, W. Wei, M.S. Chua, S. So, A.J. Butte, Reversal of cancer gene expression correlates with drug efficacy and reveals therapeutic targets, Nat. Commun. 8 (2017) 16022.
[11] C. Liu, J. Su, F. Yang, K. Wei, J. Ma, X. Zhou, Compound signature detection on LINCS L1000 big data, Mol. Biosyst. 11 (2015) 714–722.
[12] J. Li, S. Zheng, B. Chen, A.J. Butte, S.J. Swamidass, Z. Lu, A survey of current trends in computational drug repositioning, Briefings Bioinf. 17 (2016) 2–12.
[13] R.R. Shah, P.D. Stonier, Repurposing old drugs in oncology: opportunities with clinical and regulatory challenges ahead, J. Clin. Pharm. Ther. 44 (2019) 6–22.
[14] J. Lamb, E.D. Crawford, D. Peck, J.W. Modell, I.C. Blat, M.J. Wrobel, J. Lerner, J.P. Brunet, A. Subramanian, K.N. Ross, M. Reich, H. Hieronymus, G. Wei, S.A. Armstrong, S.J. Haggarty, P.A. Clemons, R. Wei, S.A. Carr, E.S. Lander, T.R. Golub, The Connectivity Map: using gene-expression signatures to connect small molecules, genes, and disease, Science 313 (2006) 1929–1935.
[15] J. Chen, M. Ma, N. Shen, J.J. Xi, W. Tian, Integration of cancer gene co-expression network and metabolic network to uncover potential cancer drug targets, J. Proteome Res. 12 (2013) 2354–2364.
[16] J. Bain, L. Plater, M. Elliott, N. Shpiro, C.J. Hastie, H. McLauchlan, I. Klevernic, J.S. Arthur, D.R. Alessi, P. Cohen, The selectivity of protein kinase inhibitors: a further update, Biochem. J. 408 (2007) 297–315.
[17] K. Clark, L. Plater, M. Peggie, P. Cohen, Use of the pharmacological inhibitor BX795 to study the regulation and physiological roles of TBK1 and IkappaB kinase epsilon: a distinct upstream kinase mediates Ser-172 phosphorylation and activation, J. Biol. Chem. 284 (2009) 14136–14146.
[18] C. Peifer, D.R. Alessi, Small-molecule inhibitors of PDK1, ChemMedChem 3 (2008) 1810–1838.
[19] L.Y. Bai, C.F. Chiu, N.P. Kapuriya, T.M. Shieh, Y.C. Tsai, C.Y. Wu, A.M. Sargeant, J.R. Weng, BX795, a TBK1 inhibitor, exhibits antitumor activity in human oral squamous cell carcinoma through apoptosis induction and mitotic phase arrest, Eur. J. Pharmacol. 769 (2015) 287–296.
[20] W. Chen, K. Luo, Z. Ke, B. Kuai, S. He, W. Jiang, W. Huang, Z. Cai, TBK1 promote bladder cancer cell proliferation and migration via akt signaling, J. Cancer 8 (2017) 1892–1899.
[21] M.T. Wang, M. Holderfield, J. Galeas, R. Delrosario, M.D. To, A. Balmain, F. McCormick, K-ras promotes tumorigenicity through suppression of non-canonical wnt signaling, Cell 163 (2015) 1237–1251.
[22] I. Kim, Y.S. Choi, J.H. Song, E.A. Choi, S. Park, E.J. Lee, J.K. Rhee, S.C. Kim, S. Chang, A drug-repositioning screen for primary pancreatic ductal adenocarcinoma cells identifies 6-thioguanine as an effective therapeutic agent for TPMT-low cancer cells, Mol Oncol 12 (2018) 1526–1539.
[23] J.L. Ali, B.J. Lagasse, A.J. Minuk, A.J. Love, A.I. Moraya, L. Lam, G. Arthur, S.B. Gibson, L.C. Morrison, T.E. Werbowetski-Ogilvie, Y. Fu, M.W. Nachtigal, Differential cellular responses induced by dorsomorphin and LDN-193189 in chemotherapy-sensitive and chemotherapy-resistant human epithelial ovarian cancer cells, Int. J. Cancer 136 (2015) E455–E469.
[24] P. Stanetty, G. Hattinger, M. Schnurch, M.D. Mihovilovic, Novel and efficient access to phenylamino-pyrimidine type protein kinase C inhibitors utilizing a Negishi cross-coupling strategy, J. Org. Chem. 70 (2005) 5215–5220.
[25] H.W. Han, S. Hahn, H.Y. Jeong, J.H. Jee, M.O. Nam, H.K. Kim, D.H. Lee, S.Y. Lee,

D.K. Choi, J.H. Yu, S.H. Min, J. Yoo, LINCS L1000 dataset-based repositioning of CGP-60474 as a highly potent anti-endotoxemic agent, Sci. Rep. 8 (2018) 14969.
[26] D. Cihalova, F. Staud, M. Ceckova, Interactions of cyclin-dependent kinase inhibitors AT-7519, flavopiridol and SNS-032 with ABCB1, ABCG2 and ABCC1 transporters and their potential to overcome multidrug resistance in vitro, Cancer Chemother. Pharmacol. 76 (2015) 105–116.
[27] R. Furst, Narciclasine - an Amaryllidaceae alkaloid with potent antitumor and anti-inflammatory properties, Planta Med. 82 (2016) 1389–1394.
[28] C. Greenhill, Metabolism: Narciclasine boosts energy metabolism, Nat. Rev. Endocrinol. 13 (2017) 189.
[29] J.F. Soderholm, S.L. Bird, P. Kalab, Y. Sampathkumar, K. Hasegawa, M. Uehara-Bingen, K. Weis, R. Heald, Importazole, a small molecule inhibitor of the transport receptor importin-beta, ACS Chem. Biol. 6 (2011) 700–708.
[30] H.P. Soares, M. Ming, M. Mellon, S.H. Young, L. Han, J. Sinnet-Smith, E. Rozengurt, Dual PI3K/mTOR inhibitors induce rapid overactivation of the MEK/ERK pathway in human pancreatic cancer cells through suppression of mTORC2, Mol. Cancer Ther. 14 (2015) 1014–1023.
[31] H.L. Vu, A.E. Aplin, Targeting TBK1 inhibits migration and resistance to MEK inhibitors in mutant NRAS melanoma, Mol. Cancer Res. 12 (2014) 1509–1519.
[32] R.E. Bachelder, S.O. Yoon, C. Franci, A.G. de Herreros, A.M. Mercurio, Glycogen synthase kinase-3 is an endogenous inhibitor of Snail transcription: implications for the epithelial-mesenchymal transition, J. Cell Biol. 168 (2005) 29–33.
[33] R. Virtakoivu, A. Mai, E. Mattila, N. De Franceschi, S.Y. Imanishi, G. Corthals, R. Kaukonen, M. Saari, F. Cheng, E. Torvaldson, V.M. Kosma, A. Mannermaa, G. Muharram, C. Gilles, J. Eriksson, Y. Soini, J.B. Lorens, J. Ivaska, Vimentin-erk signaling uncouples slug gene regulatory function, Cancer Res. 75 (2015) 2349–2362.
[34] H. Chen, G. Zhu, Y. Li, R.N. Padia, Z. Dong, Z.K. Pan, K. Liu, S. Huang, Extracellular signal-regulated kinase signaling pathway regulates breast cancer cell migration by maintaining slug expression, Cancer Res. 69 (2009) 9228–9235.